Potentiometric Ion-Selective Sensors based on UV-Ozone Irradiated Laser-Induced Graphene Electrode

Sudipta Choudhury , Soumyendu Roy , Gourav Bhattacharya , Sam Fishlock , Sujit Deshmukh , Sangita Bhowmick , James McLaughlign , Susanta Sinha Roy

PII: S0013-4686(21)00631-9
DOI: https://doi.org/10.1016/j.electacta.2021.138341
Reference: EA 138341

To appear in: *Electrochimica Acta*

Received date: 20 September 2020
Revised date: 30 March 2021
Accepted date: 3 April 2021

Please cite this article as: Sudipta Choudhury , Soumyendu Roy , Gourav Bhattacharya , Sam Fishlock , Sujit Deshmukh , Sangita Bhowmick , James McLaughlign , Susanta Sinha Roy , Potentiometric Ion-Selective Sensors based on UV-Ozone Irradiated Laser-Induced Graphene Electrode, *Electrochimica Acta* (2021), doi: https://doi.org/10.1016/j.electacta.2021.138341

Potentiometric Ion-Selective Sensors based on UV-Ozone Irradiated Laser-Induced Graphene Electrode

Sudipta Choudhury,[a] Soumyendu Roy,[b*] Gourav Bhattacharya,[c] Sam Fishlock,[c] Sujit Deshmukh,[a] Sangita Bhowmick,[a] James McLaughlign,[c] Susanta Sinha Roy,[a*]

[a] *Department of Physics, School of Natural Sciences, Shiv Nadar University, Gautam Buddha Nagar 201314, Uttar Pradesh, India*

[b] *Department of Physics, School of Engineering and Applied Sciences, Bennett University, Greater Noida 201310, Uttar Pradesh, India*

[c]*Nanotechnology and Integrated Bioengineering Centre, School of Engineering, Ulster University, Newtownabbey, Belfast BT37 0QB, Northern Ireland, United Kingdom*

AUTHOR INFORMATION

Corresponding Authors

[*]E-mail: susanta.roy@snu.edu.in ; soumyendu.roy@bennett.edu.in

Abstract

Disposable devices for sensing biomarkers like Na^+ ion in sweat was developed using UV-Ozone irradiated laser-induced graphene (LIG) based electrodes. Solid-state ion-selective electrodes (ISEs) sensitive to Na^+ ions were fabricated by a two-step drop-coating process of polyvinyl chloride solution containing plasticizer, ionophore and ion-exchanger on LIG electrode. Hydrophobic to hydrophilic transition induced by UV-Ozone treatment reduced the contact angle, resulting in better permeation of the ion-selective membrane into the ozonized LIG film. Raman spectroscopy and IR absorption studies indicate physisorption of ozone on LIG.

Performance of ozonized LIG (O-LIG) electrodes was much better than pristine LIG and screen-printed carbon electrodes. Sensitivity of 60.2 ± 0.9 mV/ decade to Na^+ ions and a lower limit of detection of 1×10^{-6} M was achieved using O-LIG based ISEs. Response time of the devices were around 1 min.

Keywords

Laser-induced graphene; ion-selective membrane; wearable electrode; electrochemical analysis; sweat sensor.

1. Introduction

In recent years, electrochemical sensors have emerged as a popular device for real-time analysis and non-invasive monitoring of human body fluids such as urine, blood, sweat, tears, saliva and interstitial fluid [1-4]. It is important to detect and quantify the concentration of biomarkers such as metabolites, proteins, antibodies, electrolytes, ions and hormones which can provide crucial information about health and physical status of a person [2, 4-8]. Analysis of sweat has drawn great attention as it contains chemical and biological markers that are responsible for many diseases and physiological disorders such as dehydration, cystic fibrosis, stress disorders, bone mineral loss, hyponatremia, osteoporosis and drug abuse [4, 8-15]. Although sweat contains a lot of pathological information, it has been neglected in healthcare diagnostics due to the technical difficulties associated with the collection and analysis of sweat [11, 16-19]. Current state of the art in ion-selective electrodes have generated hope of overcoming these hurdles through miniaturization of conventional clinical sensors [20, 21]. ISE is a combination of conducting electrode and ion-selective membrane (ISM) that can function as an electrochemical

potentiometric ion sensor. Synthesis of suitable electrode material and selection of a proper ISM is therefore utmost important for sweat analysis using the potentiometric technique.

Conventional ISEs are liquid contact electrodes which contain an ionic solution (also referred to as inner filling solution) between the electrode and the ISM [20, 22]. These liquid contact ISEs has certain limitations such as evaporation of the inner filling solution, transportation of liquid across the sensing membrane due to osmotic pressure, deviations of sample temperature and pressure [22]. This can damage the overall senor's performances. It is also extremely difficult to miniaturize liquid contact ISEs. Thus it is imperative to replace these liquid contact electrodes by solid-state ISEs [23]. Carbon-based nanomaterials like three dimensional ordered macroporous carbon, glassy carbon, carbon nanospheres, carbon nanotube, graphene and fullerene have shown tremendous promise as solid-state ISEs for electrochemical bio-sensing [24-31]. Recent development in the area of solid contact ISEs has shown that introducing a thin conducting polymer as an intermediate layer between the electrode material and sensing membrane can improve ion-to-electron transduction [32]. It is well established that graphene-based electrodes hold immense potential for electrochemical sensors owing to their high electron mobility, high electrical and thermal conductivity, mechanical flexibility and most importantly high surface area and porosity [33-35]. Despite numerous potential applications, large scale chemical-free production of porous graphene is a challenging task. Recently, a simple, scalable and cost-effective technique was developed for the synthesis of 3D porous few-layered graphene using a single-step laser-writing process [36]. Graphene synthesised by this process is usually referred to as laser-induced graphene (LIG). It has already shown promising results in numerous applications, such as electrochemical sensors, biosensors, microfluidic systems, electronic devices, catalysis, water purification etc [37-44].

One of the disadvantages of LIG is their hydrophobic nature. Coating hydrophobic LIG films with ISM is significantly difficult and results in ISEs with low sensitivity and non-repeatable performance. So, it is important to fabricate LIG with tunable wettability. Studies have shown that there can be a reversible transition between hydrophobic and hydrophilic states of graphene. Jing *et al.*[45] demonstrated that the surface wettability of graphene can be modified by various methods, one of them is ozone (O_3) treatment, which has been used in the current work to make LIG surface hydrophilic. Studies suggest that the interaction between ozone and graphene can occur in two ways: one is physisorption and the other is chemisorption [46]. Physisorption generally leads to an upshift of Dirac point and is responsible for p-type doping [47]. This decreases resistance and improves the electrical conductivity of graphene [48]. Chemisorption results in changes in the atomic structure of graphene [48]. In physisorption, ozone molecules intercalate between the layers of few-layered graphene which leads to an increase in the electrochemically active surface area and the content of turbostratic and monolayer graphene. Hence it improves the sensor performances.

In the current article, we report the improvement in ion sensing performance by using ozonized LIG (O-LIG) electrodes because of its increased electrochemical active surface area and porosity. We have shown that the ISM in solution state diffuses throughout the pores of O-LIG. After solidification, ISM forms a strong attachment to O-LIGs and enables a robust flexible ion sensing device. Hydrophilicity and high porosity of the electrode improve the penetration and attachment of ISM to the electrode, which in turn improves the transduction of electrochemical changes happening inside the ISM in presence of target ions into the electrical potential of the electrode.

2. Experimental

2.1. Synthesis of pristine and ozonized LIG (O-LIG) Electrodes

Laser-induced graphene was synthesized using a Universal Laser system over a 50 μm thick as-received Kapton polyimide (Printed electronics ltd. UK) sheet. The laser treatment was carried out in ambient atmospheric condition with the help of Universal Laser 230 VLS (CO_2 laser). For the conversion of polyimide into LIG, the laser power was kept constant at 8.1 W and the lasing speed was controlled at 570 mm s^{-1}. The electrode, along with the connection lines and pads was fabricated by laser patterning the polyimide substrate using the same protocol. The laser converts sp^3 hybridized carbon in polyimide film into sp^2 hybridized carbon [36].After fabrication, we have performed the ozone treatment of LIG in a Novascan PSD Pro Series digital UV-Ozone cleaner where the ozone is produced by ultraviolet irradiation (254 nm of UV light with an intensity of 20 mW/cm^2) in ambient conditions. The ozonization of LIG was carried out for 30 minutes at room temperature.

2.2. Material Characterization

Scanning electron microscopy (SEM) was performed using a Hitachi SU5000 and Energy-dispersive X-ray spectroscopy (EDS) data were obtained using an Oxford instrument and analyzed by using Aztec software. Raman spectroscopy was done by using a micro-Raman spectrometer (STR) equipped with a 532 nm argon-ion laser source with a power of 2.5 mW and 50× magnification objective lens. Fourier transform infrared spectroscopy (FTIR) was carried out using Nicolte iS5 FTIR spectrometer (Thermo Fisher Scientific) in attenuated-total-reflectance mode on a diamond crystal. Hydrophobicity and hydrophilicity with both water and concentrated ISM solution on LIG surfaces (before and after ozone treatment of LIG) were investigated by

static and dynamic contact angle measurements (Krüss GmbH, DSA-25). The sessile drop method was carried out by applying a droplet of 2 µL volume. Both Deionized water (Resistivity 18.2 MΩ-cm) and concentrated ISM solution were taken as test liquids.

2.3. ISM Solutions

Sodium ion-selective membrane solution comprised of 264 mg of polymer poly(vinyl chloride) (PVC) (high molecular weight, Selectophore grade, Sigma-Aldrich), 528.8 mg of plasticizer bis(2-ethylhexyl) sebacate (DOS) (purity ≥97.0%, Selectophore grade, Sigma-Aldrich), 5.6 mg of 4-tert-butycalix [4] arene-tetraacetic acid tetraethyl ester (sodium ionophore X) (Selectophore grade, Sigma Aldrich), and 1.6 mg of ion exchanger potassium tetrakis ((4-chlorophenyl)-borate (purity ≥98.0%, Selectophore grade, Sigma-Aldrich) dissolved in 10 mL of solvent tetrahydrofuran (THF; purity ≥99.9%, anhydrous, inhibitor-free, Sigma-Aldrich).[49, 50] The mixture was allowed to rest for about 5 minutes and then stirred until a pellucid solution was obtained. The concentration of this sodium ISM solution was 0.08 g/mL and henceforth in this article, it is referred to as the concentrated ISM solution. To dilute this ISM solution to a concentration of 0.008 g/mL, we added extra THF in a volume ratio of 9:1.[26]

2.4. Fabrication of ISEs

ISM coating on pristine LIG and O-LIG was prepared by a two-step drop-casting process that has been reported earlier to produce good results.[26] At first we drop coated 200 μL of dilute (0.008 g/mL) solution and then 100 μL of concentrated (0.08 g/mL) solution. Typical electrode size was 0.5 × 0.5 cm^2. A minimum 40-50 s gap was kept between two consecutive coats to allow the dilute ISM solution to permeate the LIG film. The ISM coated electrodes were kept at rest for 12 hours under ambient conditions to dry slowly. ISM was also drop coated on a screen-printed carbon electrode by using the same method. Before conducting any

characterization/measurement, the ISEs were dipped inside a 0.1 M NaCl solution for 30-40 min followed by dipping in DI water for 10-15 min. This process activates the pores on the surface of ISM and the ion-conducting channels inside the polymeric ISM.

2.5. Electrochemical Measurements

Cyclic voltammetry (CV) and measurements of open-circuit potentials (OCPs) were carried out using an Autolab potentiostat/galvanostat 302N instrument (Metrohm B.V. Utrecht, Netherlands) controlled by Nova (version 1.10) software. CV was performed using a three-electrode setup that consisted of a working electrode (LIG), Pt wire as a counter electrode, Ag/AgCl (with 3 M potassium chloride electrolyte) as a reference electrode and 1 Molar NaCl was used as the electrolyte. 15-20 cycles were recorded until at-least 5 stable and repeatable cycles were obtained. These stable cycles were considered for measuring the capacitance. OCP measurements were conducted in a two-electrode configuration with ISE as working electrode and Ag/AgCl reference electrode. Under open-circuit conditions no current is flowing in the system, hence there is no need for using the third counter electrode. OCPs were measured by dipping the electrodes in the test solutions, i.e. NaCl solutions of varying concentrations. Artificial sweat was prepared according to the European reference method EN1811:2011 by dissolving urea (0.1 wt %), lactic acid (0.1 wt %) in deionized water with varying sodium concentrations of 10^{-4} to 1M. The pH of the prepared artificial sweat solution was maintained at 6.5 ± 0.05.

The dependence of OCP (*E*) of an ISE on the concentration (*C)* of target ion in the test solution is given by the Nicolskii-Eisenman equation:

$$E = \text{constant} + \frac{2.303RT}{zF}\log C$$

Where '*R*' is the universal gas constant, '*T*' is the absolute temperature, '*z*' is the charge on the ion being detected and *'F*' is the Faraday's constant [20, 51, 52]. Here it is assumed that there are no other inferring ions. The plot of the OCP vs. log of the concentration of target ion should be a straight line with slope, $\frac{2.303RT}{zF}$. On substituting the values of these constants, the slope turns out to be 60.2 mV/decade for Na^+ ion at room temperature. The slope of the linear fit of experimentally obtained calibration curve of an ISE is termed as its sensitivity. The lower limit of detection (LOD) of an ISE was determined by following the IUPAC convention, according to which LOD is the concentration of target ion where the error of the analysis is 100% [53]. Based on the Nicolskii-Eisenman equation, we can say that at LOD the concentration of this monovalent ion is twice or half of the predicted value from the linear fitted calibration curve. Thus the difference between measured and predicted OCP at LOD is $\Delta E = \pm \frac{2.303RT}{zF}\log 2 = \pm 18$ mV, at room temperature, for monovalent ions. For estimating the linear fit to the sodium ISE calibration curves data in the range 1×10^{-4} to 1 M was used. The linear range of an ISE is defined as the part of the calibration curve where the deviations from linear fit do not exceed the standard error values [53].

3. Results and discussion

The foremost sensing element of the ISEs is ISM which comprises a plasticized polymer doped with a lipophilic complexing agent termed as ionophore [54, 55]. It is the ionophore that gives ISE its selectivity towards the specific target ion [56, 57]. The Ion-exchanger, potassium tetrakis ((4-chlorophenyl)-borate, used in the current study maintains charge neutrality of the ion-selective membrane (ISM). As Na^+ ions enter the ISM, electrostatic potential keeps building up, so it is necessary to lose some other positive charges. The K^+ ions from the exchanger go into the

test solution. Ideally, the ion-exchanger has no direct interaction with the target ions, i.e. Na^+ or other interfering ions.

In the current study, the amorphous polymer matrix was prepared by mixing PVC with DOS. The amorphous nature improves ion conductivity. In order to construct an ISE for sodium, sodium selective neutral ionophore (Na-X) and ion exchanger potassium tetrakis ((4-chlorophenyl) borate were incorporated in the polymeric matrix [49, 50]. Sodium ionophore X has a high sensitivity to Na^+ ion and superior selectivity against other similar ions like H^+, K^+ and NH_4^+ [50, 58, 59]. We examined selectivity measurements using O-LIG based Na^+ ISEs. The selectivity of the Na^+ ISE towards K^+ ion (log $K^{pot}_{Na,K}$) was calculated by separate solution method (SSM) [60] (for 10^{-3} M solutions) and was found to be -2.31± 0.23, which is comparable to values reported in the literatures.[60-63]. Potentiometric selectivity co-efficient is given by the Nicolsky–Eisenman equation [64]

$$E = E_0 + R\,T / (z_A\,F) \ln [a_A + \sum_B K_{A,B}^{pot}\,(a_B)^{z_A/z_B}]$$

where, E is the measured potential; E_0 is a reference potential; z_A and z_B are the charge on the primary ion, A and interfering ion B; a_A and a_B are the activities of the primary ion, A, and the interfering ion B; $K_{A,B}^{pot}$ is the potentiometric selectivity co-efficient for the primary ion A against the interfering ion, B; R, T and F are universal gas constant, the absolute temperature and the Faraday's constant.

Using Nicolsky–Eisenman equation selectivity coefficient can be expressed as:

$$\log K_{A,B}^{pot} = \frac{(E_B - E_A)\,z_A\,F}{RT \ln 10} + (1 - z_A/z_B) \log a_A$$

which is equivalent to

$$K_{A,B}^{pot} = a_A^{\left(1-{}^{z_A}/_{z_B}\right)}\ e^{(E_\mathrm{B}-E_\mathrm{A})\,z_A\,F/RT}$$

where E_A is the measured potential of a pure solution of primary ion and E_B is the measured potential of a pure solution of the interfering ion at the same activity.

The O-LIG was prepared by direct laser scribing on polyimide films followed by UV-ozone treatment. By this treatment, ozone molecules are physisorbed on the LIG surface [47].

This converted the hydrophobic surface of LIG into hydrophilic, which was further confirmed by water contact angle (WCA) analysis (Fig. 1a and 1b). The contact angle decreases from 123° to 0° after the UV-ozone treatment. The hydrophilic surface of O-LIG allows easier penetration of ISM solution into the LIG film, thus creating a strong attachment of the ISM membrane to O-LIG film and ensuring proper electrical connectivity between the two layers.

ISM was drop-coated onto the O-LIG based electrodes in a two-step drop coating process to fabricate the ISEs. Electrochemical measurements were done to study the sensing performance of the ISEs using a potentiostat/galvanostat. The OCP measurements were done with two-electrode systems, where the electrodes were dipped in NaCl solution and the concentration of this solution was changed from 10^{-6} to 1 M in multiplicative steps of 10. OCPs at the ISEs were measured with Ag/AgCl as a reference electrode. The concentration of Na^+ ions in human sweat lies in the range 10^{-4} to 1 M [65], this includes extreme physiological condition like dehydration. OCP data within this range was fitted with straight lines to produce the calibration curves. The average sensitivity of O-LIG based ISEs was found to be 60.2 ± 0.9 mV/decade, a typical calibration curve is shown in Fig. 2a and for pristine LIG based ISE it was found around 42.7 ± 0.9 mV/decade (Fig. 2b). Comparing the error bars in the two figures we can see that the repeatability of the OCP measurements with O-LIG electrodes is significantly better. Also, the OCPs of this ISE were stable for one hour. Linear response of O-LIG based ISEs was found in

the range of 1×10^{-6} to 1 M. Working range of the ISEs was also from 10^{-6} to 1 M, with the lower limit of detection being 10^{-6} M. Average response time of the sensor was about one minute and is primarily due to the time needed by the Na^+ ions to diffuse through the membrane and set up an equilibrium potential. A typical time response of the sensors is shown in Fig. 2c.

Fig. 3. shows the results of cyclic voltammetry (CV) measurements conducted in a 1 M NaCl solution with pristine and O-LIG (without ISM coating electrodes) at a scan rate of 150 mV/s with a potential window from -0.1 V to +0.6 V (*vs*. Ag/AgCl). We see that there is a significant increase in current for O-LIG electrode as compared to its pristine counterpart. The areal specific capacitance was estimated to be 4.8 μF/cm^2 for the pristine LIG electrode. After the ozone treatment, approximately 9-fold enhancement in the specific capacitance for the O-LIG electrode was observed and a specific capacitance of 42.4 μF/cm^2 was estimated. The areal specific capacitances were calculated from the CV loops according to the following equation:[66, 67]

$$C = \oint IdV / (2Av\Delta V)$$

Where C is the areal specific capacitance (μF cm^{-2}), $\oint IdV$ is the area of CV loop, A is the electrode area in cm^2, v is the scan rate (mV s^{-1}) and ΔV is the potential window (V).

LIG films and ISEs were characterized by scanning electron microscopy (SEM), energy dispersive x-ray spectroscopy (EDS), Raman spectroscopy and fourier transform infrared spectroscopy (FTIR). SEM was used to assess the surface morphology of both pristine LIG (Fig. 4a and 4b) and O-LIG (Fig. 4c and 4d). After ozone treatment, the flaky LIG surface with sharp protrusion-like features is converted to a rough surface with fewer protrusions. This change in morphology can also reduce contact angles with liquid surfaces and reduce hydrophobicity.

The concentration of ISM solutions plays an important role during fabrication of ISEs and was also found to have a strong effect on the sensor's performance [26]. As reported earlier [26],

ISEs with best sensitivity (60.2 ± 0.9 mV/decade) and stability were obtained by following a two-step drop-coating process. The first step involves coating O-LIG electrodes based ISEs with a dilute (0.008 g/mL) ISM solution, which is followed by a second coat of concentrated (0.08 g/mL) ISM solution. Coating with only dilute or concentrated solution of ISM results in ISEs with poor performance. From the contact angle (CA) measurement (Fig. S1, Supplementary Data) it can be seen that ISM solution drops have smaller contact angle with the surface of O-LIG films as compared to pristine LIG. So, the ISM solution is able to penetrate the O-LIG films more efficiently. From cross-sectional SEM (Fig. 4e) one can see evidence of penetration and strong attachment between the ISM layer and O-LIG film. The composition and recipe for making ion-selective membrane and electrode were adapted from previously reported procedures [49,68-70]. The primary criterion used in these articles for optimizing the fabrication process is to check whether the ISEs showed a Nernstian response towards the sodium ion concentration. The ISEs in the current study were prepared using these previously reported procedures and exhibited near Nernstian response with varying concentration of NaCl solution over a range of 10^{-4} to 1M. Hence no further optimization was performed.

The presence of clear chlorine signal in the EDS spectrum (Fig. 5) indicates the presence of PVC inside the O-LIG films and thus confirms the penetration of ISM.

The sensitivity of ISEs based on screen-printed carbon electrodes (Fig. S2, Supplementary Data) was found to be lower than O-LIG based electrodes. Attachment of ISM to printed carbon films is much weaker as compared to the attachment to LIG films and it can be easily peeled off from the surface. Thus, we can conclude that the O-LIG with high porosity and enhanced hydrophilicity can make better contact with ISM than other metals or carbon films. The strong attachment coupled with the networked structure of thin sheet-like and ribbon-like graphene

films in LIG creates a robust and flexible sensing device that can resist usual mechanical distortions. Higher capacitance of O-LIG films implies more electrochemical interfacial area with ISM and improved transduction of changes in concentration of Na^+ coordinated ionophores to electrical potential of the ISE. Higher capacitance of electrodes is also known to stabilize signals in potentiometric sensing [28]. The electrochemical active surface area (EASA) (Fig. S3 and Fig. S4Supplementary Data) was also calculated for both types of LIG electrodes. O-LIG has higher (70.8 mm^2) EASA than pristine LIG (6.11 mm^2) of same geometric size. The increased EASA of O-LIG, allows easier transduction from electrochemical to electrical potential. It is also quite evident that the hydrophobic to hydrophilic transition by ozone treatment has contributed to the high EASA [71]. Stability and reproducibility tests of sodium ion selective electrodes were carried out and the results are included in the revised manuscript. The O-LIG based ISE showed good reproducibility (Fig. 6a) across 5 different individual ISEs with an average sensitivity of 63.6 mV/decade and a standard deviation of 2.4%. Long-term stability (Fig. 6b) of the sensors, over a period of 4 weeks, was also studied. The result indicates that the sodium ion sensor can maintain its sensitivity with minimal loss. Reproducibility and stability of these Na^+-ISEs indicate that it can be used for continuous and real time monitoring of sodium content in sweat.

Raman spectroscopy is an important tool to study the structure of graphene-based materials [72, 73]. Fig. 7a shows the Raman spectrum of both LIG surfaces before and after ozone treatment. In case of pristine LIG the prominent D, G and 2D peaks appear at ~1343 cm^{-1}, ~1576 cm^{-1} and ~2677 cm^{-1}. For O-LIG the above bands appear at ~1345 cm^{-1}, ~1580 cm^{-1} and 2682 cm^{-1} respectively. D peak represents the breathing mode of k-point phonon of A_{1g} symmetry.[74] G peak indicates E_{2g} phonon of sp^2 hybrid carbon atoms.[72] 2D peak is an overtone of D peak (two phonons lattice vibration) [75]. Its position and shape indicates graphene layer thickness

and doping level of graphene [76]. The intensity ratio of D to G band [I_D/I_G] for O-LIG sample increased slightly from 0.92 to 1.05 compared to untreated sample. This indicates that some additional defects in the sp^2 lattice of LIG were introduced by UV-ozone treatment. This defects could be created due to the knocking-out of C atoms from graphene lattice by the bombardment of ozone ions, creation of Stone-Wales defects and removal of the passivating H atoms at the edges of the graphene flakes, thereby exposing more dangling bonds. UV-ozone treatment can also induces oxygen functional groups in the edge planes of LIG. However, this is not a major factor here as indicated by the FTIR study shown below. The increase in I_D signal could also be due to the simple fact that ozone treatment reduces the protruding graphene layers (see figures 4 (a) and (c)) bringing more edge C atoms within the small 3D focal region of the Raman laser. The small increase in I_D/I_G ratio also indicates that the defect formation is restricted to a minimum possible level, thus not adversely affecting the electrical conductivity of the LIG film. Also, for pristine LIG and O-LIG the intensity ratio of the 2D to G band [I_{2D}/I_G] was almost same (0.67 and 0.64). This means the no. of layers in both LIG samples are almost identical (few layer graphene). FTIR spectroscopy (Fig. 7b) was performed to study the chemical nature of LIG before and after ozone treatment. For both the samples we got the presence of bands corresponding to C-O at 1090 cm^{-1}, C-O-C at 1237 cm^{-1}, C-OH at 1374 cm^{-1} and C=O at 1709 cm^{-1}. Among these, the peaks at 1090 cm^{-1} and 1374 cm^{-1} can be related to hydroxyl, carbonyl and epoxy groups [66]. The presence of 1237 cm^{-1} and 1709 cm^{-1} peaks can be ascribed to ketone and epoxide groups on the surface of LIG samples [77]. This confirms that ozone treatment is a physisorption process, does not alter the atomic structure nor does it introduce any oxygen-containing functional groups. This conclusion is further strengthened by the observation that the

conversion of LIG surface from hydrophobic to hydrophilic is a temporary effect and the surface regains most of its hydrophobicity with time.

We have investigated the detection of Na^+ ions in EN1811:2011 artificial sweat solution [78]. The response of the Na^+-ISEs in the artificial sweat is displayed in Fig. 8a and 8b. The data demonstrate the feasibility of using the electrodes for testing real sweat. The average sensitivity of the O-LIG based ISE in artificial sweat was found to be 65.8 ± 1.3 mV/decade. Also, the reproducibility of the sensor was tested with artificial sweat and the data is shown in Fig. 8c. The high sensitivity, reproducibility and stability of the electrode indicate that it can serve as a non-invasive wearable sensing platform for personal health monitoring.

Overall, the current study demonstrates that the LIG-based electrodes can be used as a flexible electrochemical sensing platform and is particularly suitable as an ISE.

4. Conclusions

A stable solid contact ion selective sweat sensor was developed using laser-induced graphene (LIG) as the electrode material. Ozone treatment was found to improve the attachment of ISM to LIG resulting in improved device performance parameters like sensitivity, stability and reliability. SEM, CV, ECSA, contact angle, Raman and FTIR spectroscopy shows that modification in surface morphology and improved hydrophilicity caused by ozone physisorption are the primary causes of improvement in ISE performance. The best sensitivity of the ISEs was found to be 60.2 ± 0.9 mV/decade. Sensitivity, response time, LOD and working range of the ISEs indicate that we can use LIG based sensors as noninvasive wearable devices in the future for applications like sweat sensing.

References

[1] A.J. Bandodkar, J. Wang, Non-invasive wearable electrochemical sensors: a review, Trends Biotechnol. 32 (2014) 363-371.

[2] A. Ganguly, S. Prasad, Passively Addressable Ultra-Low Volume Sweat Chloride Sensor, Sensors, 19 (2019) 4590.

[3] T. Kaya, G. Liu, J. Ho, K. Yelamarthi, K. Miller, J. Edwards, A. Stannard, Wearable sweat sensors: background and current trends, Electroanalysis, 31 (2019) 411-421.

[4] J. Kim, A.S. Campbell, B.E.-F. de Ávila, J. Wang, Wearable biosensors for healthcare monitoring, Nat. Biotechnol. 37 (2019) 389-406.

[5] P. Pirovano, M. Dorrian, A. Shinde, A. Donohoe, A.J. Brady, N.M. Moyna, G. Wallace, D. Diamond, M. McCaul, A wearable sensor for the detection of sodium and potassium in human sweat during exercise, Talanta, (2020) 121145.

[6] P. Pirovano, A. Shinde, P. White, G. Wallace, M. McCaul, D. Diamond, Real-time Analysis of Electrolytes in Sweat Through a Wearable Sensing Platform, Multidisciplinary Digital Publishing Institute Proceedings, 2019, pp. 14.

[7] S. Robinson, A.H. Robinson, Chemical composition of sweat, Physiol. Rev. 34 (1954) 202-220.

[8] Q. Zhai, L.W. Yap, R. Wang, S. Gong, Z. Guo, Y. Liu, Q. Lyu, J. Wang, G.P. Simon, W. Cheng, Vertically Aligned Gold Nanowires as Stretchable and Wearable Epidermal Ion-Selective Electrode for Noninvasive Multiplexed Sweat Analysis, Anal. Chem. 92 (2020) 4647-4655.

[9] K. Mitsubayashi, M. Suzuki, E. Tamiya, I. Karube, Analysis of metabolites in sweat as a measure of physical condition, Anal. Chim. Acta 289 (1994) 27-34.

[10] A. Lynch, D. Diamond, M. Leader, Point-of-need diagnosis of cystic fibrosis using a potentiometric ion-selective electrode array, Analyst, 125 (2000) 2264-2267.

[11] M. Beauchamp, L. Lands, Sweat-testing: A review of current technical requirements, Pediatr. Pulmonol. 39 (2005) 507-511.

[12] N. De Giovanni, N. Fucci, The current status of sweat testing for drugs of abuse: a review, Curr. Med. Chem. 20 (2013) 545-561.

[13] M.H. Rosner, J. Kirven, Exercise-associated hyponatremia, Clin. J. Am. Soc. Nephrol. 2 (2007) 151-161.

[14] A.H. Marques, M.N. Silverman, E.M. Sternberg, Evaluation of stress systems by applying noninvasive methodologies: measurements of neuroimmune biomarkers in the sweat, heart rate variability and salivary cortisol, Neuroimmunomodulation, 17 (2010) 205-208.

[15] M. Bergeron, Heat cramps: fluid and electrolyte challenges during tennis in the heat, J Sci Med Sport , 6 (2003) 19-27.

[16] S.T. Keene, D. Fogarty, R. Cooke, C.D. Casadevall, A. Salleo, O. Parlak, Wearable Organic Electrochemical Transistor Patch for Multiplexed Sensing of Calcium and Ammonium Ions from Human Perspiration, Adv. Healthc. Mater. 8 (2019) 1901321.

[17] S. Shirreffs, R. Maughan, Whole body sweat collection in humans: an improved method with preliminary data on electrolyte content, J. Appl. Physiol. 82 (1997) 336-341.

[18] V.A. LeGrys, Assessment of sweat-testing practices for the diagnosis of cystic fibrosis, Arch. Pathol. Lab. Med. 125 (2001) 1420-1424.

[19] A. Mishra, R. Greaves, J. Massie, The relevance of sweat testing for the diagnosis of cystic fibrosis in the genomic era, The Clinical biochemist. Clin Biochem Rev 26 (2005) 135.

[20] J. Bobacka, A. Ivaska, A. Lewenstam, Potentiometric ion sensors, Chem. Rev. 108 (2008) 329-351.

[21] J.R. Windmiller, J. Wang, Wearable electrochemical sensors and biosensors: a review, Electroanalysis, 25 (2013) 29-46.

[22] I.S. Kucherenko, D. Sanborn, B. Chen, N. Garland, M. Serhan, E. Forzani, C. Gomes, J.C. Claussen, Ion-Selective Sensors Based on Laser-Induced Graphene for Evaluating Human Hydration Levels Using Urine Samples, Adv. Mater. Technol. (2020) 1901037.

[23] T. Han, U. Mattinen, J. Bobacka, Improving the sensitivity of solid-contact ion-selective electrodes by using coulometric signal transduction, ACS sensors, 4 (2019) 900-906.

[24] F. Li, J. Ye, M. Zhou, S. Gan, Q. Zhang, D. Han, L. Niu, All-solid-state potassium-selective electrode using graphene as the solid contact, Analyst, 137 (2012) 618-623.

[25] L. Zhao, Y. Jiang, H. Wei, Y. Jiang, W. Ma, W. Zheng, A.-M. Cao, L. Mao, In Vivo Measurement of Calcium Ion with Solid-State Ion-Selective Electrode by Using Shelled Hollow Carbon Nanospheres as a Transducing Layer, Anal. Chem. 91 (2019) 4421-4428.

[26] S. Roy, M. David-Pur, Y. Hanein, Carbon nanotube-based ion selective sensors for wearable applications, ACS Appl. Mater. Interfaces 9 (2017) 35169-35177.

[27] P. Ramnani, N.M. Saucedo, A. Mulchandani, Carbon nanomaterial-based electrochemical biosensors for label-free sensing of environmental pollutants, Chemosphere, 143 (2016) 85-98.

[28] M.A. Fierke, C.-Z. Lai, P. Buhlmann, A. Stein, Effects of architecture and surface chemistry of three-dimensionally ordered macroporous carbon solid contacts on performance of ion-selective electrodes, Anal. Chem. 82 (2010) 680-688.

[29] R. Hernández, J. Riu, F.X. Rius, Determination of calcium ion in sap using carbon nanotube-based ion-selective electrodes, Analyst, 135 (2010) 1979-1985.

[30] A. Düzgün, A. Maroto, T. Mairal, C. O'Sullivan, F.X. Rius, Solid-contact potentiometric aptasensor based on aptamer functionalized carbon nanotubes for the direct determination of proteins, Analyst, 135 (2010) 1037-1041.

[31] M. Fouskaki, N. Chaniotakis, Fullerene-based electrochemical buffer layer for ion-selective electrodes, Analyst, 133 (2008) 1072-1075.

[32] J. Hu, A. Stein, P. Bühlmann, Rational design of all-solid-state ion-selective electrodes and reference electrodes, Trends Analyt Chem 76 (2016) 102-114.

[33] M.G. Stanford, K. Yang, Y. Chyan, C. Kittrell, J.M. Tour, Laser-induced graphene for flexible and embeddable gas sensors, ACS nano, 13 (2019) 3474-3482.

[34] N.T. Garland, E.S. McLamore, N.D. Cavallaro, D. Mendivelso-Perez, E.A. Smith, D. Jing, J.C. Claussen, Flexible laser-induced graphene for nitrogen sensing in soil, ACS Appl. Mater. Interfaces 10 (2018) 39124-39133.

[35] Q. He, S.R. Das, N.T. Garland, D. Jing, J.A. Hondred, A.A. Cargill, S. Ding, C. Karunakaran, J.C. Claussen, Enabling inkjet printed graphene for ion selective electrodes with postprint thermal annealing, ACS Appl. Mater. Interfaces 9 (2017) 12719-12727.

[36] J. Lin, Z. Peng, Y. Liu, F. Ruiz-Zepeda, R. Ye, E.L. Samuel, M.J. Yacaman, B.I. Yakobson, J.M. Tour, Laser-induced porous graphene films from commercial polymers, Nat. Commun. 5 (2014) 1-8.

[37] R. Ye, D.K. James, J.M. Tour, Laser-induced graphene, Acc. Chem. Res. 51 (2018) 1609-1620.

[38] P. Nayak, N. Kurra, C. Xia, H.N. Alshareef, Highly efficient laser scribed graphene electrodes for on-chip electrochemical sensing applications, Adv. Electron. Mater. 2 (2016) 1600185.

[39] L.-Q. Tao, H. Tian, Y. Liu, Z.-Y. Ju, Y. Pang, Y.-Q. Chen, D.-Y. Wang, X.-G. Tian, J.-C. Yan, N.-Q. Deng, An intelligent artificial throat with sound-sensing ability based on laser induced graphene, Nat. Commun. 8 (2017) 1-8.

[40] F. Tehrani, B. Bavarian, Facile and scalable disposable sensor based on laser engraved graphene for electrochemical detection of glucose, Sci. Rep. 6 (2016) 1-10.

[41] C. Fenzl, P. Nayak, T. Hirsch, O.S. Wolfbeis, H.N. Alshareef, A.J. Baeumner, Laser-scribed graphene electrodes for aptamer-based biosensing, ACS sensors, 2 (2017) 616-620.

[42] D.C. Vanegas, L. Patiño, C. Mendez, D.A.d. Oliveira, A.M. Torres, C.L. Gomes, E.S. McLamore, Laser scribed graphene biosensor for detection of biogenic amines in food samples using locally sourced materials, Biosens. 8 (2018) 42.

[43] S. Sharma, S.K. Ganeshan, P.K. Pattnaik, S. Kanungo, K.N. Chappanda, Laser induced flexible graphene electrodes for electrochemical sensing of hydrazine, Mater. Lett. 262 (2020) 127150.

[44] A.C. Marques, A.R. Cardoso, R. Martins, M.G.F. Sales, E. Fortunato, Laser-Induced Graphene-Based Platforms for Dual Biorecognition of Molecules, ACS Appl. Nano Mater. 3 (2020) 2795-2803.

[45] J. Feng, Z. Guo, Wettability of graphene: from influencing factors and reversible conversions to potential applications, Nanoscale Horiz 4 (2019) 339-364.

[46] N. Leconte, J. Moser, P. Ordejon, H. Tao, A. Lherbier, A. Bachtold, F. Alsina, C.M. Sotomayor Torres, J.-C. Charlier, S. Roche, Damaging graphene with ozone treatment: a chemically tunable metal− insulator transition, ACS nano, 4 (2010) 4033-4038.

[47] S. Jandhyala, G. Mordi, B. Lee, G. Lee, C. Floresca, P.-R. Cha, J. Ahn, R.M. Wallace, Y.J. Chabal, M.J. Kim, Atomic layer deposition of dielectrics on graphene using reversibly physisorbed ozone, ACS nano, 6 (2012) 2722-2730.

[48] J. Yuan, L.-P. Ma, S. Pei, J. Du, Y. Su, W. Ren, H.-M. Cheng, Tuning the electrical and optical properties of graphene by ozone treatment for patterning monolithic transparent electrodes, ACS nano, 7 (2013) 4233-4241.

[49] A.J. Bandodkar, D. Molinnus, O. Mirza, T. Guinovart, J.R. Windmiller, G. Valdés-Ramírez, F.J. Andrade, M.J. Schöning, J. Wang, Epidermal tattoo potentiometric sodium sensors with wireless signal transduction for continuous non-invasive sweat monitoring, Biosens. Bioelectron. 54 (2014) 603-609.

[50] A. Cadogan, Z. Gao, A. Lewenstam, A. Ivaska, D. Diamond, All-solid-state sodium-selective electrode based on a calixarene ionophore in a poly (vinyl chloride) membrane with a polypyrrole solid contact, Anal. Chem. 64 (1992) 2496-2501.

[51] P. Bühlmann, L.D. Chen, Ion-selective electrodes with ionophore-doped sensing membranes, Supramolecular Chemistry: From Molecules to Nanomaterials, (2012).

[52] E. Bakker, P. Bühlmann, E. Pretsch, Carrier-based ion-selective electrodes and bulk optodes. 1. General characteristics, Chem. Rev. 97 (1997) 3083-3132.

[53] K.N. Mikhelson, Ion-selective electrodes, Springer2013.

[54] E. Bakker, P. Bühlmann, E. Pretsch, Polymer Membrane Ion-Selective Electrodes–What are the Limits?, Electroanalysis: An International Journal Devoted to Fundamental and Practical Aspects of Electroanalysis, 11 (1999) 915-933.

[55] E. Bakker, E. Pretsch, P. Bühlmann, Selectivity of potentiometric ion sensors, Anal. Chem. 72 (2000) 1127-1133.

[56] E.E. Totu, C. Spatarelu, A. Maier, Ion-Selective Polymeric Membranes for Chemical Sensors. I, stress, 3 (2009) 4.

[57] R. Canovas, S. Padrell Sánchez, M. Parrilla, M. Cuartero, G.A. Crespo, Cytotoxicity study of ionophore-based membranes: Toward on-body and in vivo ion sensing, ACS sensors, 4 (2019) 2524-2535.

[58] Y. Shibutani, H. Yoshinaga, K. Yakabe, T. Shono, M. Tanaka, Polymeric membrane sodium-selective electrodes based on calix [4] arene ionophores, Calixarenes 50th Anniversary: Commemorative Issue, Springer1994, pp. 333-342.

[59] P. Bühlmann, E. Pretsch, E. Bakker, Carrier-based ion-selective electrodes and bulk optodes. 2. Ionophores for potentiometric and optical sensors, Chem. Rev. 98 (1998) 1593-1688.

[60] A. M. Cadogan, D. Diamond, M. R. Smyth, M. Deasy, M. A. McKervey, S. J. Harris, Sodium-selective polymeric membrane electrodes based on calix [4] arene ionophores. Analyst, 114 (1989), 1551-1554.

[61] Q. Zhai, L. W. Yap, R. Wang, S. Gong, Z. Guo, Y. Liu, W. Cheng, Vertically aligned gold nanowires as stretchable and wearable epidermal ion-selective electrode for noninvasive multiplexed sweat analysis. Anal. Chem. 92 (2020), 4647-4655.

[62] J. Zhu, X. Li, Y. Qin, Y. Zhang, Single-piece solid-contact ion-selective electrodes with polymer–carbon nanotube composites. Sensors and Actuators B: Chemical 148 (2010), 166-172.

[63] M. Parrilla, I. Ortiz-Gómez, R. Canovas, A. Salinas-Castillo, M. Cuartero, A.G. Crespo, Wearable potentiometric ion patch for on-body electrolyte monitoring in sweat: Toward a validation strategy to ensure physiological relevance. Anal. Chem. 91(2019), 8644-8651.

[64] Y. Umezawa, P. Bühlmann, K. Umezawa, K. Tohda, S. Amemiya, Potentiometric selectivity coefficients of ion-selective electrodes. Part I. Inorganic cations (technical report). Pure and Applied Chemistry, 72 (2000), 1851-2082.

[65] C.J. Harvey, R.F. LeBouf, A.B. Stefaniak, Formulation and stability of a novel artificial human sweat under conditions of storage and use, Toxicol In Vitro 24 (2010) 1790-1796.

[66] Y. Zhao, J. Liu, B. Wang, J. Sha, Y. Li, D. Zheng, M. Amjadipour, J. MacLeod, N. Motta, Supercapacitor electrodes with remarkable specific capacitance converted from hybrid graphene oxide/NaCl/urea films, ACS Appl. Mater. Interfaces 9 (2017) 22588-22596.

[67] H. Raha, B. Manna, D. Pradhan, P.K. Guha, Quantum capacitance tuned flexible supercapacitor by UV-ozone treated defect engineered reduced graphene oxide forest, Nanotechnology, 30 (2019) 435404.

[68] W. Gao, S. Emaminejad, H.Y.Y. Nyein, S. Challa, K. Chen, A. Peck, A. Javey, Fully integrated wearable sensor arrays for multiplexed in situ perspiration analysis. Nature, 529 (2016), 509-514.

[69] W. He, C. Wang, H. Wang, M. Jian, W. Lu, X. Liang, Y. Zhang, Integrated textile sensor patch for real-time and multiplex sweat analysis. Sci. Adv. 5 (2019), eaax0649.

[70] Q. An, S. Gan, J. Xu, Y. Bao, T. Wu, H. Kong, L. Niu, A multichannel electrochemical all-solid-state wearable potentiometric sensor for real-time sweat ion monitoring. Electrochem. commun., 107 (2019), 106553.

[71] J. Zhang, M. Ren, L. Wang, Y. Li, B.I. Yakobson, J.M. Tour, Oxidized Laser-Induced Graphene for Efficient Oxygen Electrocatalysis, Adv. Mater. 30 (2018) 1707319.

[72] M.E. Uddin, R.K. Layek, N.H. Kim, D. Hui, J.H. Lee, Preparation and properties of reduced graphene oxide/polyacrylonitrile nanocomposites using polyvinyl phenol, Composites Part B: Engineering, 80 (2015) 238-245.

[73] Z. Xu, Z. Ao, D. Chu, A. Younis, C.M. Li, S. Li, Reversible hydrophobic to hydrophilic transition in graphene via water splitting induced by UV irradiation, Sci. Rep. 4 (2014) 1-9.

[74] P. Khanra, M.E. Uddin, N.H. Kim, T. Kuila, S.H. Lee, J.H. Lee, Electrochemical performance of reduced graphene oxide surface-modified with 9-anthracene carboxylic acid, RSC Adv.5 (2015) 6443-6451.

[75] S. Roscher, R. Hoffmann, O. Ambacher, Determination of the graphene–graphite ratio of graphene powder by Raman 2D band symmetry analysis, Anal. Methods 11 (2019) 1224-1228.

[76] H. Sun, D. Chen, Y. Wu, Q. Yuan, L. Guo, D. Dai, Y. Xu, P. Zhao, N. Jiang, C.-T. Lin, High quality graphene films with a clean surface prepared by an UV/ozone assisted transfer process, J. Mater. Chem. C 5 (2017) 1880-1884.

[77] A.K. Das, M. Srivastav, R.K. Layek, M.E. Uddin, D. Jung, N.H. Kim, J.H. Lee, Iodide-mediated room temperature reduction of graphene oxide: a rapid chemical route for the synthesis of a bifunctional electrocatalyst, J. Mater. Chem. A 2 (2014) 1332-1340.

[78] K. Midander, A. Julander, J. Kettelarij, C. Lidén, Testing in artificial sweat–is less more? Comparison of metal release in two different artificial sweat solutions. Regulatory Toxicology and Pharmacology, 81(2016), 381-386.

Figure Captions

Fig. 1. Water contact angle measurements and wettability of surfaces of (a) Pristine LIG and (b) O-LIG (UV-ozone treated) on polyimide film.

Fig. 2. Sensor performance. Calibration curve of (a) Ozone-treated and (b) pristine LIG-based ISE. The concentration of test solution was changed from 1×10^{-6} to 1 M in a stepwise manner. This measurement was performed with a standard Ag/AgCl reference electrode. (c) Time response graph of O-LIG based ISE. All OCPs were measured using a potentiostat.

Fig. 3. Cyclic voltammograms of pristine LIG and O-LIG electrodes in 1 M NaCl (aqueous) electrolyte at a constant scan rate of 150 mV/s.

Fig. 4. SEM images (a,b) of pristine LIG. (c,d) Ozone treated LIG. (e) Cross-sectional SEM image of ISE prepared by two-step drop-coating process showing the different layers. (f) SEM image showing the porous morphology of the top surface of an ISE.

Fig. 5. EDS spectrum from LIG after drop-coating of ISM, confirming the percolation of ISM into the LIG film.

Fig. 6. (a) Reproducibility and (b) stability study of the sodium ion sensors.

Fig. 7. (a) Raman spectra of pristine LIG and O-LIG showing the characteristic peaks associated with sp^2 hybridized honeycomb lattice of graphene. (b) FTIR spectra of pristine LIG and O-LIG showing absorption from various bonds present in the material.

Fig. 8. Electrochemical performance of the Na^+ sensors in artificial sweat. (a) Calibration curve of sodium sensors with increasing sodium concentration (10^{-4} to 1 M). (b) The open-circuit potential responses of the sensors. (c) Reproducibility of the sensors in artificial sweat.

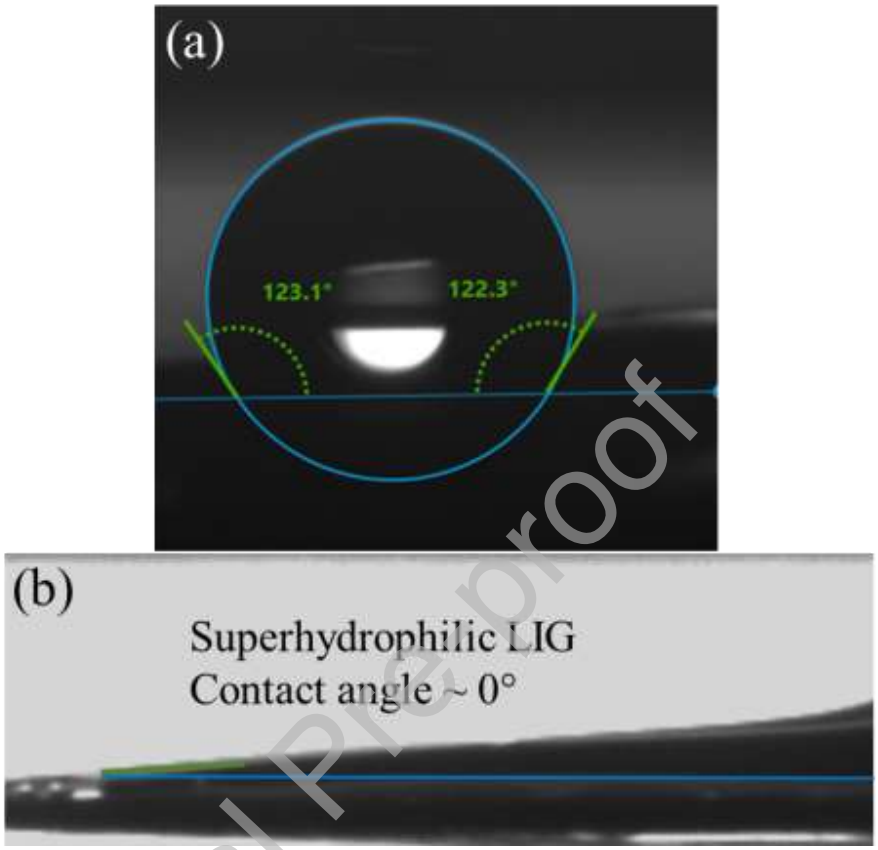

Fig. 1.

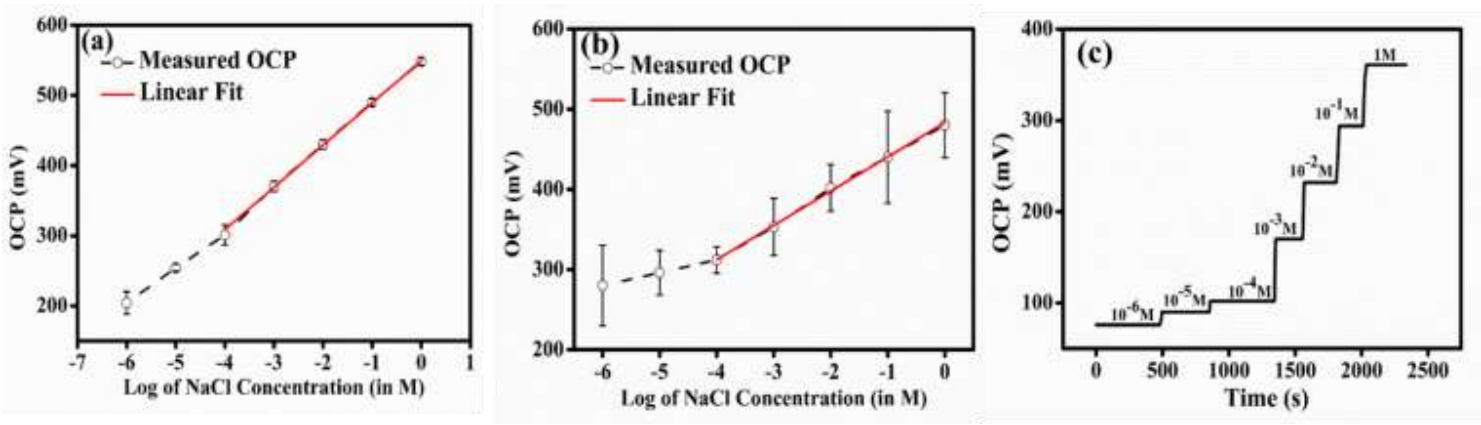

Fig. 2.

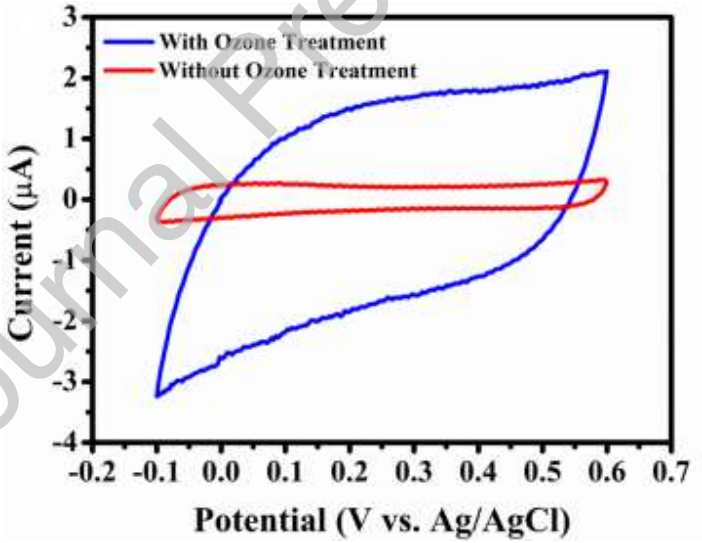

Fig. 3.

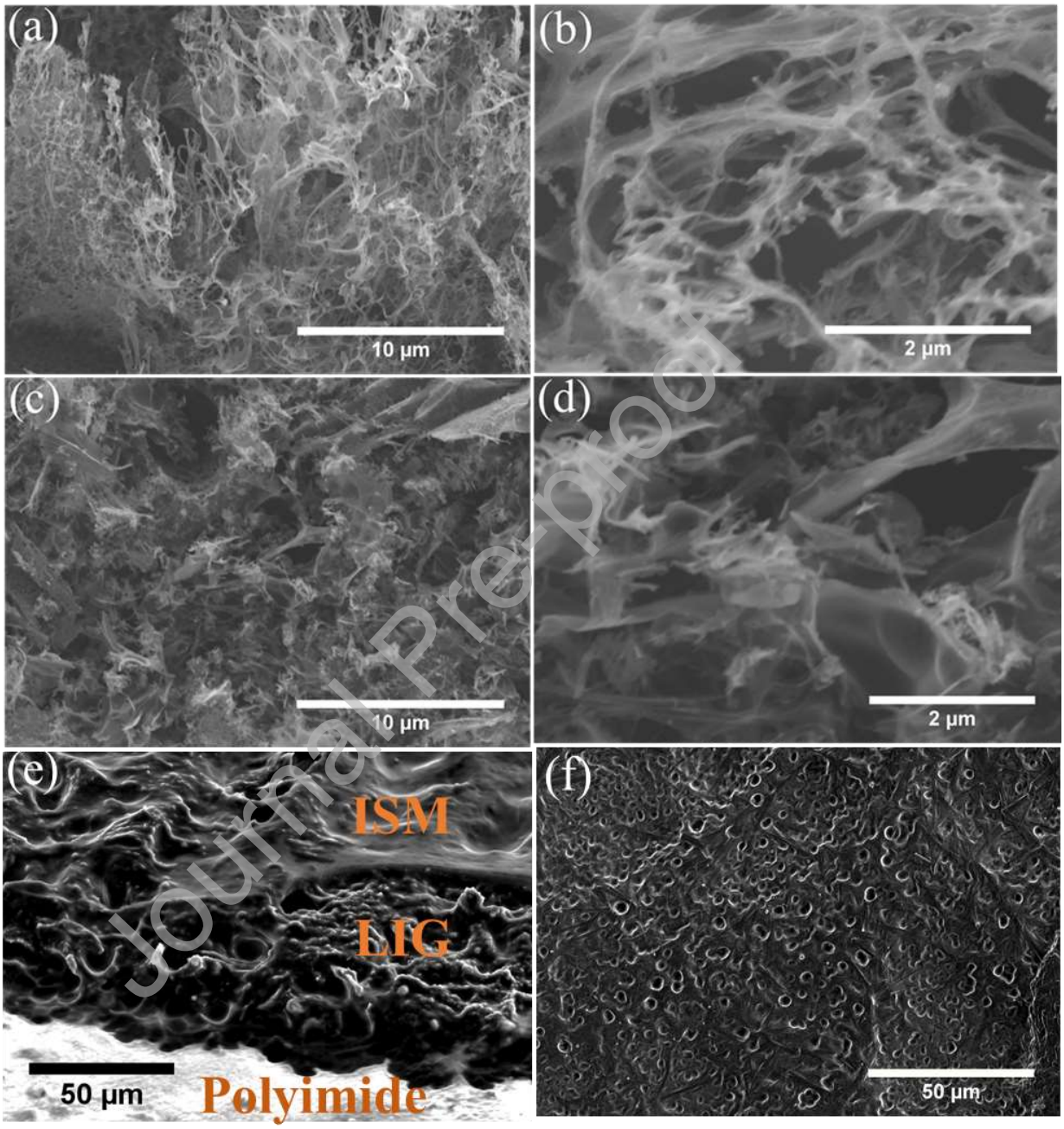

Fig. 4.

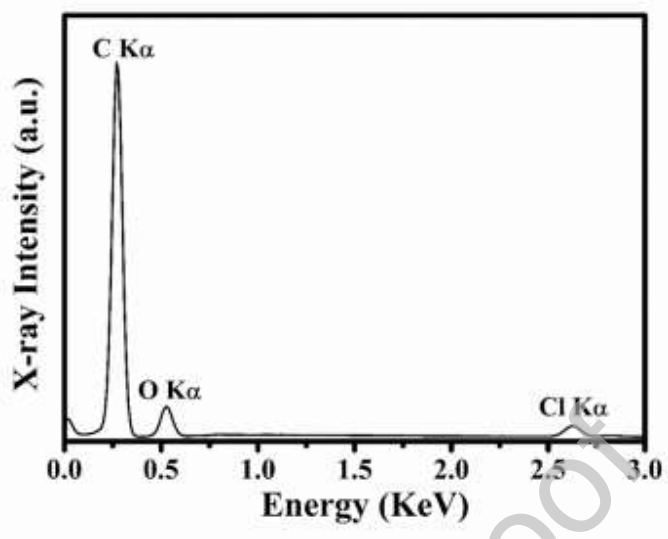

Fig. 5.

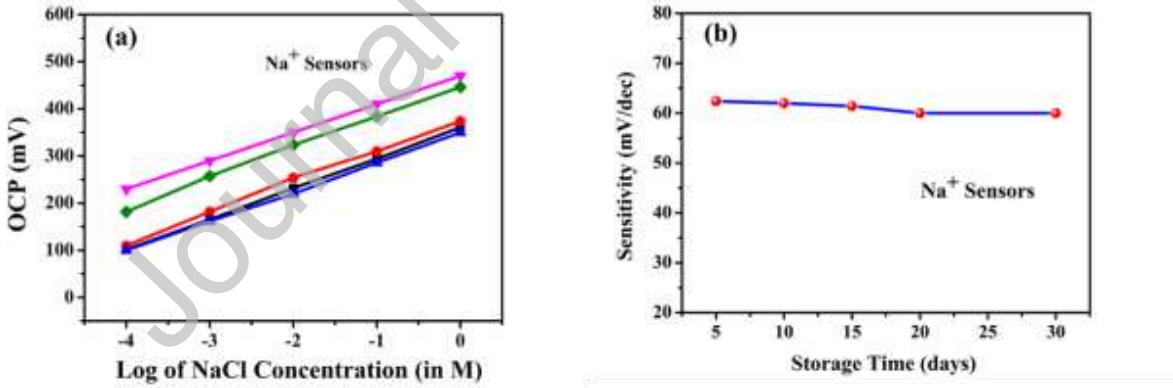

Fig. 6.

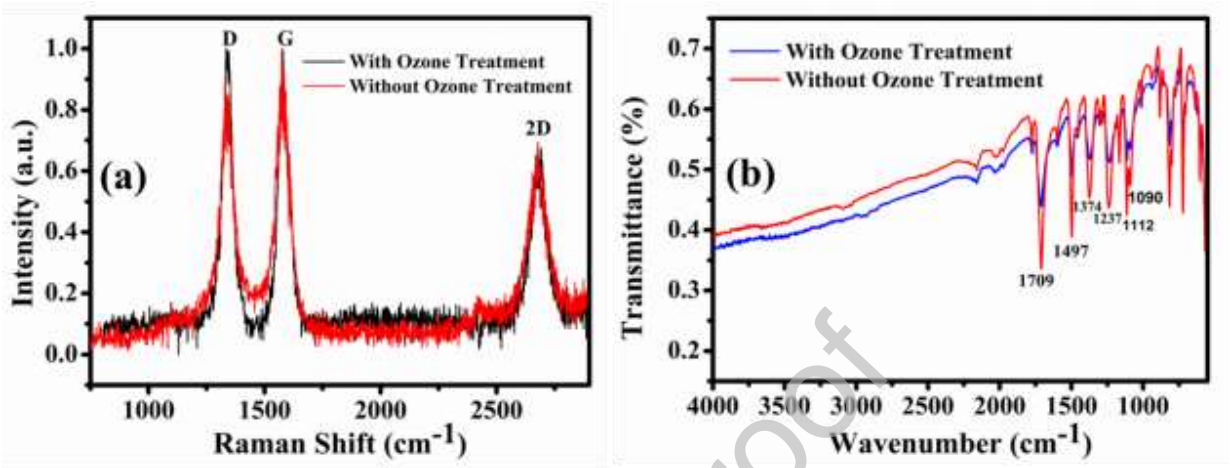

Fig. 7.

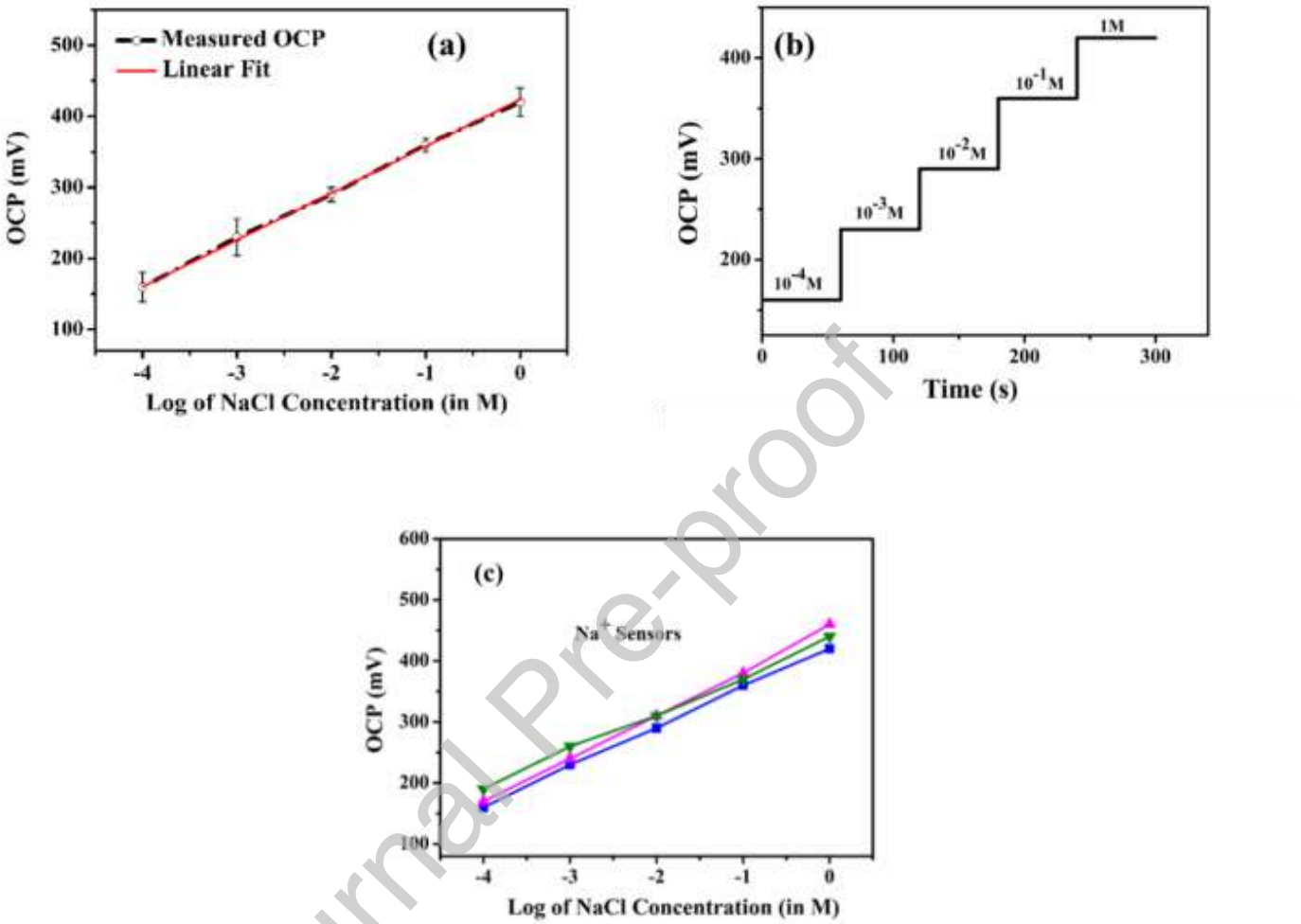

Fig. 8.